Phonon modes and central peaks in an *A*-site relaxor: A low-frequency Raman study of sodium bismuth titanate

Daniel K. Jackson* and Jean Toulouse
Department of Physics, Lehigh University, Bethlehem, Pennsylvania 18015, USA

Haosu Luo
Shanghai Institute of Ceramics, Chinese Academy of Sciences, Shanghai 201800, China
(Received 14 June 2013; revised manuscript received 6 July 2014; published 14 August 2014)

Raman spectroscopic measurements of sodium bismuth titanate ($Na_{0.5}Bi_{0.5}TiO_3$ or NBT) were carried out upon cooling from 1000 to 80 K to study its two phase transitions. Full spectral deconvolution was performed, comparing the results from several fitting models, with a particular emphasis on the evolution of the central peak and low-frequency phonon modes. The central intensity profile is found to be composed of two well-defined Lorentzian peaks, the temperature dependence of which suggests the presence of fluctuations in *M*-point and *R*-point rotations of the oxygen octahedra as well as cation displacements related to polar nanodomains. The temperature behavior of both central peaks is discussed in relation to the (tilting or shifting) transition behavior in similar perovskite systems. The four observed low-frequency phonon modes indicate a different symmetry assignment than the commonly assigned $R3c$ for the low-temperature phase.

DOI: 10.1103/PhysRevB.90.054108 PACS number(s): 78.30.Hv, 63.20.dd, 77.80.Jk, 64.70.K−

I. INTRODUCTION

Sodium bismuth titanate ($Na_{0.5}Bi_{0.5}TiO_3$ or NBT) is a particularly interesting relaxor system for three reasons. First, it is lead-free, with an electromechanical d_{33} coefficient for doped ceramics and solid solutions ranging from 125 to 2000 pC/N [1,2] while the single crystal ones are approximately 65 pC/N [3]. It is therefore a promising material for transducer and actuator applications as this higher-end value is close to that of the commonly used relaxor $Pb(Zn(1/3)Nb(2/3))O_{3-x}PbTiO_3$ (PZN-PT). Second, bismuth is one of the least toxic heavy metals. Third, NBT is also interesting from a condensed matter physics point of view because it exhibits, in a single system, the two major instabilities (tilting and shifting) that are separately observed in other perovskite systems. The tilting instability involves the rotation of the anion octahedra which is known to reduce the size of the unit cell [4] in the plane of the rotation, causing local strain [5]. This tilting instability gives rise to the observation of *R*- and *M*-point Bragg peaks in neutron scattering spectra [6,7] and is useful in describing the elastic domain ordering. A recent review of NBT [8] discusses the local elastic organization at several length scales: 1–2 nm platelets [9], nanometer scale twinning, and micrometer scale domains [10]. The dynamical behavior of these elastic domains is not well understood, but the slow nature of the phase transitions revealed by x-ray diffraction measurements [11] suggest there may be a time dependency of an elastic nature. This nonpolar tilting instability is also found in order-disorder fluoroperovskites such as $RbCaF_3$ [12] and $KMnF_3$ [13] as well as in oxides such as $SrTiO_3$ [14], providing useful comparisons. The shifting instability is due to cation displacements which are assumed to have polar character due to the aliovalency of the cations. The cations have been shown to be off center from their equilibrium sites at all temperatures [7], but recent studies using nuclear magnetic resonance (NMR) [15] and x-ray absorption fine structure (XAFS) [16] suggest that both the Na^{1+} and Bi^{3+} ions have multiple potential well sites in the [111] directions. The correlated motion of the cations is confirmed by the appearance of the characteristic frequency dispersion of the dielectric constant that is typical of relaxors [17], which have a Vogel-Fulcher character when doped [18] and also exhibit first-order phase transitions [19]. Nanoscale local regions with polar ordering are known as polar nanodomains (PND's), and their reorientation is understood to be the origin of the relaxor behavior. Spontaneous polarization resulting from cation displacement appears in NBT [17] below 570 K, as also seen in displacive titanate perovskites such as $BaTiO_3$ [20] and $PbTiO_3$ [21]. The experimentally determined displacement direction of the cations in the [111] direction [7] in NBT has also been confirmed by recent theoretical work on *A*-site disorder in multiferroic materials [22,23]. However, the nature of the coupling between the *A*-site cations and the rotation of the TiO_6 octahedra is poorly understood and still a topic of active research [24,25]. These PNDs can be expected to contribute to the dynamical properties if local cation reordering results in a time-dependent shifting of the cations in adjacent unit cells and may explain the slow time-dependent evolution of the dielectric constant [11].

NBT undergoes two separate transitions, a high-temperature transition at ∼820 K, from a cubic, paraelectric, paraelastic $Pm3m$ phase [7,26] to a tetragonal $P4bm$ phase, and a second lower transition around 570 K to either a rhombohedral $R3c$ or a monoclinic Cc phase [27,28]. The higher-temperature transition corresponds to antiparallel cation displacements [7] and antiferrodistortive or cog-wheel rotations of the anion octahedrons [6], described in Glazer [4] notation as $a^0a^0c^+$. The dielectric frequency dispersion is present approximately 100 K above and persists through the high-temperature transition and down to the lower-temperature one. The lower-temperature transition is a ferroelectric one that corresponds to both $a^-a^-a^-$ octahedral tilts and parallel

*daniel.k.jackson.42.dj@gmail.com

cation [111] displacements. When measured while drifting the temperature, the dielectric constant around this lower transition exhibits a thermal hysteresis which is due to the coexistence of both phases [11] but no frequency dispersion [17,29]. The results cited suggest that both transitions are not purely polar or purely structural but have mixed characters, with strain and polarization coupled and competing [30,31]. Similarities have, in fact, been noted between NBT and two other well-known relaxors, $PbMg_{\frac{1}{3}}Nb_{\frac{2}{3}}O_3$ (PMN) [30] and $PbSc_{\frac{1}{2}}Ti_{\frac{1}{2}}O_3$ (PST) [17], in which both polarization and strain play important roles.

Raman spectroscopy is a very useful tool for the study of both the lattice dynamics of the phonons and the local dynamics of the PNDs in relaxors. Making use of the symmetry-related selection rules for phonons, it also provides structural information about local symmetry changes and phase transformations. In ferroelectrics, particularly relaxors, one can distinguish between two main sections of the Raman spectrum, high frequency and low frequency. Above approximately 100 cm^{-1}, the hard phonon modes correspond to more local vibrations involving specific atoms and molecular bonds in the unit cell, and their frequencies are usually not strongly temperature dependent. At frequencies below 100 cm^{-1}, the spectrum usually contains contributions from more collective modes such as the soft optic phonon, acoustic phonons, and local relaxations that may be coupled to these phonons. These low-frequency excitations are more difficult to study, first because they are close to the intense Rayleigh line and, second, because their respective contributions overlap significantly in the frequency spectrum. The low-frequency range of the Raman spectra of relaxors and other disordered systems undergoing phase transformations is often dominated by a "central peak" (CP) associated with relaxing fluctuations or precursor dynamics of the lower-temperature phase. In relaxors such as NBT, the CP associated with these relaxations can extend significantly beyond 100 cm^{-1}, overlapping with a few of the higher-frequency phonons.

Several Raman studies of NBT have already been reported on ceramics [32], pure crystals, [30,33–35], and powders under high pressure [26,36–38], but there still are many unresolved questions. The correct symmetry of the low-temperature phase [27] and thus the total number of phonon modes associated with it, the correct temperature evolution of the soft mode, the number and origin of the CPs [33], inconsistencies in the temperature dependence of the intensity [35,39], and the mechanism of strain dynamics in NBT [40,41] are all still open questions. The previous NBT Raman studies most relevant for the present work are those of the higher-frequency region of the spectrum by Kreisel *et al.* [36] and Luo *et al.* [35] and the lower-frequency region by Siny *et al.* [30]. As already mentioned, because of the overlap of features in different regions of the spectrum, especially the CP, it is important when deconvoluting the spectra to include all peaks present rather than analyze them separately. In the present paper, we have measured full spectra up to 1000 cm^{-1} over the entire temperature range from 1000 down to 80 K and have performed a comprehensive analysis over the entire spectral range. Based on this analysis, we describe the quantitative evolution of the different low-frequency modes, propose an interpretation of the transitional behavior of NBT, and examine its concordance with earlier interpretations. Our results reveal the existence of two CP's, a narrow one and a broad one, and their respective temperature evolution provides information on the pretransitional or precursor dynamics of NBT and the nature of the two transitions.

II. EXPERIMENT

Raman measurements were carried out on a $2 \times 2 \times 0.86$ mm sample of NBT crystal grown by the top-seeded solution growth method [42] and cut with the top face normal to the (001) direction and the sides normal to the (110) directions. It was subsequently polished to optical quality and mounted in a Cryo Industries RC-102 cryofurnace between two 1.8-mm quartz plates to allow good thermal conduction and provide electrical isolation. The cryofurnace was evacuated down to approximately 10 mTorr. The Raman spectra were measured with a Horiba JY U1000 double monochromator in a 90° geometry with a frequency resolution of 1.84 cm^{-1}. During the scans, the shutter was closed in the region $\sim\pm 2$ cm^{-1} to avoid saturation of the detector. The beam from a 514.5-nm argon ion laser was launched normal to one of the faces of the crystal, i.e., along a cubic or pseudocubic axis, and polarized normal to the plane of incidence. Spectral profiles obtained at different launch points into the crystal were found to be identical, indicating homogeneity. However, spectral profiles were also identical when the laser was launched along different crystalline directions and with different polarizations, thus preventing an analysis of phonon anisotropy. The previously mentioned structural disorder involving nanometer scale platelets and twinning is believed to be responsible for both the polarization scrambling of the scattered beam and the very strong Rayleigh scattering observed at temperatures below 600 K. As a result, only unpolarized spectra were collected at different temperatures between 80 and 1000 K upon cooling and all spectra were obtained after the crystal was allowed to equilibrate for 20 minutes at each temperature.

A slight darkening of the crystal from a light yellow to a burnt amber color was also observed after exposure to 10 mW of laser power at temperatures above 570 K. Higher laser powers up to 400 mW, if used at high temperatures, darkened the crystal completely to a black color and no Raman signal was then obtainable. The darkening under 10 mW incident power increased after each subsequent heating cycle, but a 1 hour annealing treatment in air at 600 K, i.e., in the tetragonal phase, was found to bleach the crystal and restore its transparency. Therefore each measurement cycle was begun after an air anneal at 600 K to obtain the largest Raman signal possible and all measurements shown in the paper were subsequently made with a low laser power of 10 mW. Since it has not been uniformly reported by all authors, we must conclude that such darkening depends on the particular crystal studied [29,33,35].

In addition to the increased darkening resulting from repeated laser exposure, fluorescence was also observed when the crystal was exposed to 488-nm laser light. This was further investigated by measuring the optical absorption with a Perkin-Elmer Lambda 9 spectrophotometer. Figure 1 shows an optical density profile of NBT after annealing in air, and this result is qualitatively similar to the as-received samples from the crystal provider. Two absorption peaks, both with a

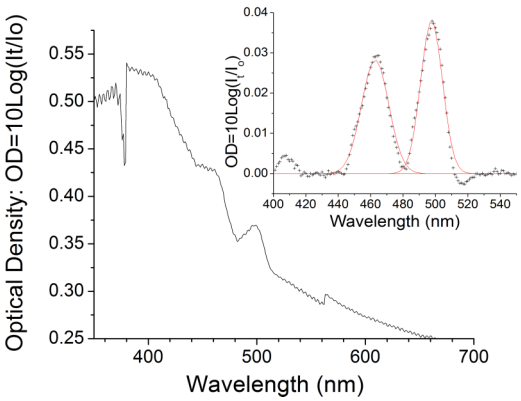

FIG. 1. (Color online) Absorbance measurement of NBT immediately after annealing the crystal in air at 600 K on a hot plate. The inset shows the two Gaussian peaks at 463 and 498 nm, which remain after subtraction of the background from the UV resonance.

Gaussian profile, are seen between 440 and 520 nm, which is different from the previously published results [3]. Due to this fluorescence, the anti-Stokes intensities were found to be anomalously larger than the Stokes ones for Raman spectra obtained with shorter excitation wavelengths (467, 488, and 501 nm). To minimize any fluorescence contribution to the Raman profiles, all measurements were therefore made with the 514.5-nm line of the laser.

Both Stokes and anti-Stokes spectra were taken at all temperatures to determine the precise internal temperature of the crystal and compare it to the measured PT100 sensor temperature. The internal temperature can be obtained by taking the ratio of the Stokes and anti-Stokes intensities. To compare the spectral profile intensities at different temperatures, a correction must be made for the thermal occupancy of the phonons, known as the Bose factor, which modifies the anti-Stokes component of a phonon by $n(\omega) = (e^{(\frac{\hbar\omega}{k_B T})} - 1)^{-1}$ and the Stokes component by $n(\omega) + 1$. The ratio $\frac{I_{\text{Stokes}}}{I_{\text{anti-Stokes}}} \approx \frac{\omega^4_{\text{Stokes}}}{\omega^4_{\text{anti-Stokes}}} \frac{n(\omega)+1}{n(\omega)} = e^{(\frac{\hbar\omega}{k_B T})}$, can be plotted as a function of frequency. The results of this analysis are shown in Fig. 2 and

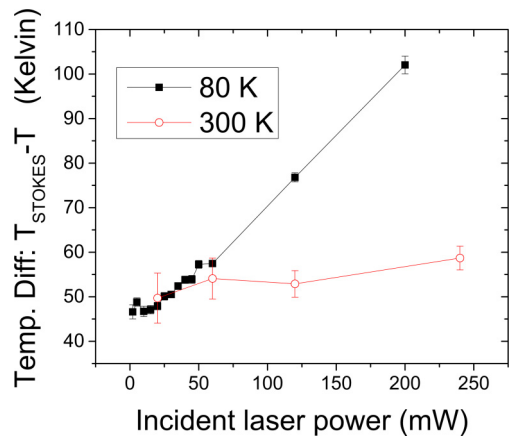

FIG. 2. (Color online) Analysis of the variation of actual crystal temperature as determined by the Stokes ratio temperature from the measured sensor temperature. The 80 and 300 K data are shown with error bars.

they reveal substantial thermal heating at 80 K for all laser powers above 2 mW but becoming negligible near 400 K, where the laser heating contribution was no longer measurable. The apparent failure of the temperature difference to approach zero as the power approaches zero is anomalous, but appears to be independent of temperature and may be due to a frequency-independent background noise. Corrections for the spectrometer grating efficiency and photomultiplier tube (PMT) quantum efficiency were taken into account but did not resolve the difference. Despite fluctuations in the Stokes/anti-Stokes ratios, the spectral profiles at each temperature were relatively consistent, staying within 5% of the original value over 8 hours of continuous laser exposure. Based on these observations the listed temperatures on all subsequent figures are the sensor temperatures of the PT100 platinum sensor. It should also be noted that precise temperature values are not critical for this study as the main focus is on the progressive temperature evolution of the profiles through each of the three crystal phases.

III. RESULTS

Figures 3(a) and 3(b) show the unpolarized Raman spectra of NBT measured at different temperatures upon cooling from 1000 K. In these spectra, one can distinguish the high-frequency peaks above ∼100 cm^{-1} from the low-frequency ones, including two CPs and a composite phonon peak centered near ∼50 cm^{-1}. The evolution of the central intensity is highlighted in Fig. 3(a), where two CPs are observed around zero frequency at all temperatures, one narrow and the other very broad, extending past 300 cm^{-1}. The narrow CP is small in the 1000 K spectra, but increases steadily in strength with decreasing temperature to a maximum amplitude at 600 K, and becomes small or is absent near 80 K. The broad peak is the dominant feature at high temperature, but progressively disappears below ∼550 K while several low-frequency phonon peaks become apparent at ∼20, ∼35, ∼50, and ∼70 cm^{-1}, as determined from the fits below. The Rayleigh peak is seen at the center of the spectrum, indicated by the abrupt rise in intensity. The high-frequency first-order phonon peaks above 100 cm^{-1}, shown in Fig. 3(b) are already observable at 1000 K, possibly due to the precursor regions of the $P4bm$ space group [43,44]. Upon cooling below 550 K, these peaks develop structure (multiple components) and their positions appear to shift towards higher frequencies as indicated by the vertical lines. This shift is due to the unequal growth of the different underlying component peaks [35].

Figure 4(b) shows the total integrated intensities as a function of temperature upon heating from 200 K or cooling from either 800 or 1000 K. The differences in the curves, while striking, have been previously reported for different NBT crystals upon cooling [39] and heating [35]. All results were obtained on the same sample and were broadly reproducible. The intensity differences between heating and cooling may therefore be a consequence of thermal hysteresis, darkening, and intrinsic structural changes. Due to these effects, all measurements shown were made either upon heating or upon cooling from the specific temperatures listed. Figure 4(a) shows the comparison of integrated intensity of the full Stokes spectrum data cooled from 1000 K to the low-frequency CPs from 5 to 50 cm^{-1} and the Bose normalized high-frequency phonon peaks above

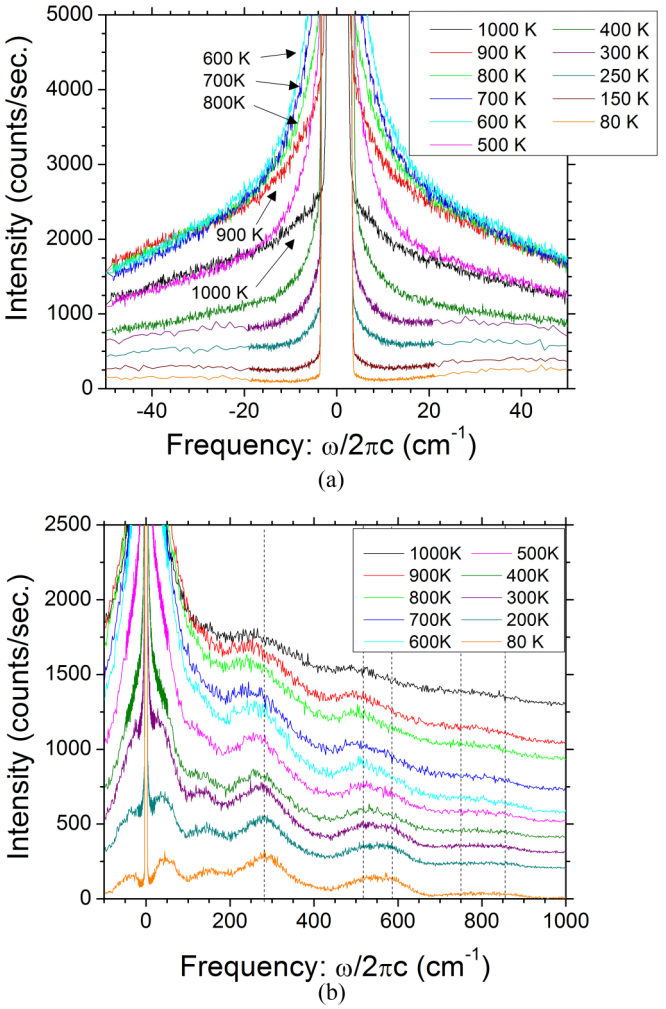

FIG. 3. (Color online) NBT Raman spectra of different frequency regions upon cooling, with vertical lines as guides for the eye to the positions of the high-frequency peaks. (a) Central peaks, (b) Full Raman spectrum.

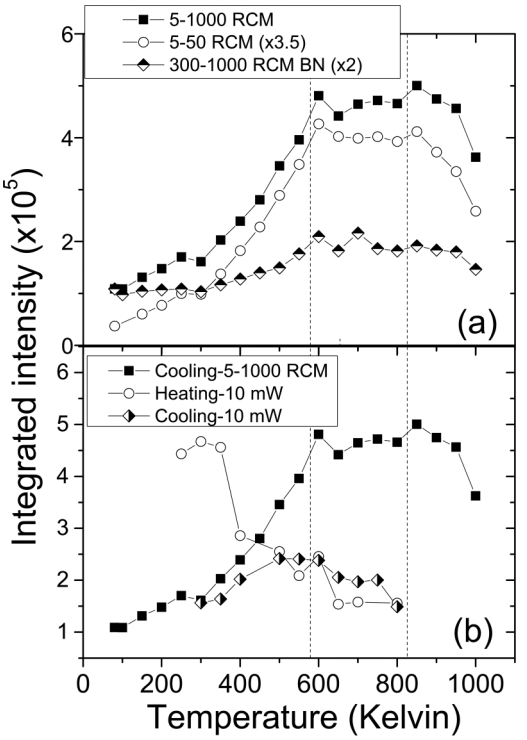

FIG. 4. (a) Comparison of the integrated intensity of different portions of the spectrum to the total integrated intensity of the cooling scan started at 1000 K, note the scaling factors in the legend. The 300–1000 cm^{-1} segment of the spectrum is shown after Bose normalization to be much less temperature dependent. (b) Integrated intensity of the Stokes portion of the spectrum for three scans from 5–1000 cm^{-1} upon heating and cooling. Integrated intensity is dependent on thermal history. The vertical lines indicate the nominal phase transition temperatures.

300 cm^{-1}. The flat portion of the 5–1000 cm^{-1} curve in the tetragonal phase is inconsistent with the expected increase in phonon density with temperature and must be attributed to a relaxation contribution. A correction by the Bose factor would cause the temperature-corrected intensity to decrease through the tetragonal phase, a result that is inconsistent with the expected temperature corrected phonon density. The decrease in intensity of the 5–50 cm^{-1} portion of the spectrum below 600 K is similar to the full 5–1000 cm^{-1} spectrum, indicating that most of this decrease is due to the CP's, which must therefore be due to relaxations and should not therefore be Bose normalized. The Bose-normalized intensity above 300 cm^{-1} is flat in the low-temperature phase below 300 K and from 650 to 950 K as would be expected based on Raman theory [45], which states that the intensity is proportional to the number of scattering centers. The increase from 350 K to a maximum at 600 K coincides with the temperature region in which the rhombohedral and tetragonal phases coexist [11].

Figure 5 shows the ratios of the raw data measured peak intensities from Fig. 3(b) upon heating and cooling for the primary peaks at 35 and 515 cm^{-1} relative to 295 cm^{-1}. Ratios of the peak intensities are seen to be the same upon cooling and heating, and therefore independent of crystal thermal history. Direct comparison of CP's, phonon widths, and phonon positions between the heating and cooling cycles are also in qualitative agreement, but the data are not shown. It is on this basis that the peak positions and widths are analyzed for their temperature dependence, regardless of the overall absolute intensity. The 295/35 peak ratios are nearly temperature independent above 550 K as seen in Fig. 5(a) but increases at lower temperatures, concurrent with the loss of integrated intensity seen in Fig. 4. This indicates that the 35 cm^{-1} is decreasing in amplitude with decreasing temperature as can be observed directly in Fig. 3(b). The 295/515 peak ratio shows an increase with decreasing temperature in the cubic phase (850–1000 K), is flat in the tetragonal phase, and has a small but steady increase in the low-temperature phase with decreasing temperature. Since apart from the usual Bose thermal population dependence, the broad CP is the spectral feature that is most rapidly changing with temperature, it is reasonable to attribute the difference in ratio behavior to the varying degrees of overlap of the CP with phonon peaks. The 35 and 295 cm^{-1} peaks in the spectrum will therefore be strongly affected by

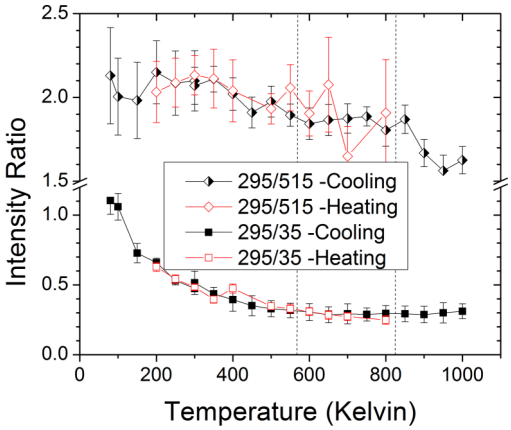

FIG. 5. (Color online) Peak intensity ratios relative to the 295 cm^{-1} peak using data without correction by Bose factor. The intensities used are directly read from the peaks of the measured spectra at the specified frequencies, using an average value and error which includes the adjacent five point values. The vertical dashed lines indicate the nominal phase transition temperatures.

changes in the broad CP while the 515 cm^{-1} and higher peaks will not, resulting in a more gradual change of the 295/515 ratios. The absence of change with the 295/35 ratios in the cubic and tetragonal phases indicates that they are affected equally by the broad CP and there is no difference between them across the phase transitions. A similar analysis was performed on the data that were completely Bose corrected as shown in Fig. 6 and the analysis where only the phonon peaks were Bose corrected as shown in Fig. 7. The results were qualitatively similar, indicating that the Bose correction is not the cause of this temperature evolution of the peak ratios. The results of the 295/135, and 295/750 peak ratios are similar to the 35 and 515 ratios and the data are not shown.

For a quantitative analysis of the temperature evolution it is convenient to correct the phonon part of the spectra by the Bose factor as explained in the experimental section, thus removing any temperature dependence related to the phonon

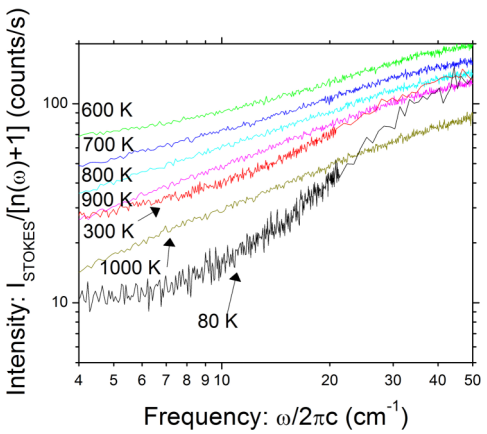

FIG. 6. (Color online) The low-frequency portion of the Raman spectrum after normalization of the spectra by dividing each data point with the Bose factor $n(\omega) + 1$. The data clearly have a temperature dependence.

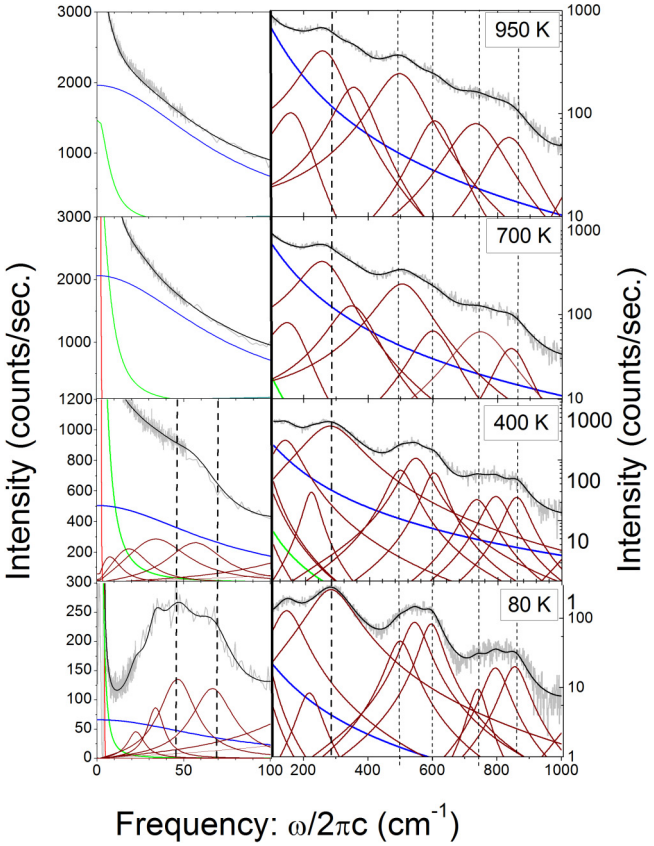

FIG. 7. (Color online) Fitted spectra at 950, 700, 400, and 78 K from the cooling data starting from 1000 K. At all temperatures, the CPs are fitted with two Lorentzian functions (blue for the broad CP and green lines for the narrow CP). High-frequency peaks are fitted with DHOs. For graphical purposes, the spectra are shown in two frequency panels, the left side has the lower frequency with linear vertical scale and the right-hand side has the higher frequencies with the log 10 vertical scale. The vertical dashed lines are visual guides to highlight the apparent shift in frequency of the peaks with temperature.

population. To demonstrate that the CPs should not be Bose corrected, Fig. 6 shows the same data from Fig. 3(a) after Bose correction has been applied to both the phonons and CPs. The corrected total intensity exhibits a strong temperature dependence at low frequency which is not consistent with the theory of phonon strength in a given structural phase. This result confirms the presence of additional scattering, which is therefore quasi-elastic and due to relaxations below ~50 cm^{-1}, similar to Raman data in disordered glass materials [46]. The temperature dependence that remains after Bose correction can then only be due to dynamical changes in the internal state of the crystal system.

IV. ANALYSIS

As explained in the experiments section, the generic expression describing Raman spectra in crystals is $I(\omega) = \{^{n(\omega)+1}_{n(\omega)}\}\mathrm{Im}\chi(\omega)$. In this expression, $\mathrm{Im}\chi(\omega)$ is the imaginary part of the susceptibility and $n(\omega)$ is the Bose thermal population factor defined previously, with $n(\omega) + 1$ for Stokes

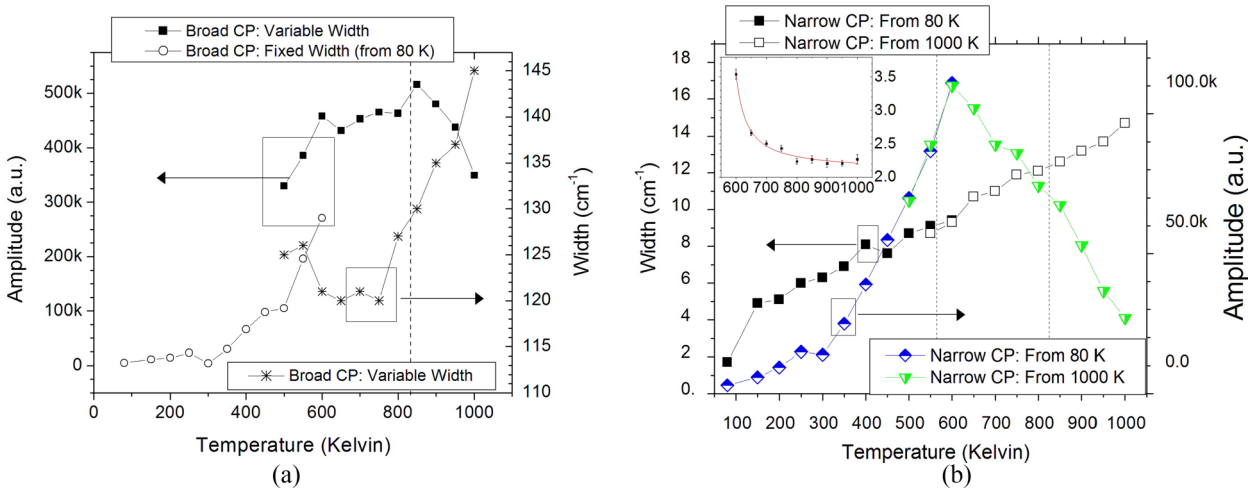

FIG. 8. (Color online) Temperature dependence of the two CP parameters of width and amplitude, showing the fits started from 80 K and 1000 K. The broad CP was fixed at 145 cm^{-1} for all low-temperature fits shown as explained in the text. Although there appears to be a discontinuity in amplitude of the broad CP, the reader should refer to Fig. 4(b) where the addition of the amplitudes of the low-frequency peaks makes up for the change in total amplitude. The inset in Fig. 8(b) is the relaxation time, $\tau = 1/c\Gamma(\times 10^{-12}\ \mathrm{s}^{-1})$, vs. temperature in Kelvin with a Vogel-Fulcher fit to the data.

processes and $n(\omega)$ for anti-Stokes processes. For phonons, the susceptibility is usually taken to be the response of a damped harmonic oscillator and the Bose factor correction is notationally modified to be $n(\omega_{0i})$ so that the entire lineshape of each ith phonon is corrected by the same correction value [45,47,48]. The Raman literature commonly fits the central and damped harmonic oscillator (DHO) peaks with $n(\omega)$, which is only really appropriate for the central peak if it is considered as a distribution of many harmonic oscillators. For relaxations, a Debye response is represented by a Lorentzian function without the Bose correction

$$\chi''(\omega) = [n(\omega_{0i}) + 1]A\omega_{0i}^2 \times \frac{\omega\Gamma}{\left(\omega_{0i}^2 - \omega^2\right)^2 + (\omega\Gamma)^2} \quad \text{DHO profile,} \qquad (1)$$

$$\chi''(\omega) = \frac{2A}{\pi}\frac{\Gamma}{\omega^2 + \Gamma^2} \quad \text{Lorentz profile,} \qquad (2)$$

where A is the integrated intensity, Γ is the damping parameter which is approximately equal to the half width at half max (HWHM) for a DHO and exactly so for a Lorentzian, and ω_{0i} is the normal frequency of the ith phonon. Due to the overlap of CPs and low-frequency modes at temperatures near the 570-K transition, the Raman spectra of NBT were analyzed in the following way while excluding the region from ± 5 cm^{-1}: Starting from the 1000-K spectral profile of the cooling data, the two CPs were initialized first with Lorentzian functions, then the high-frequency peaks, associated with hard phonons, were initialized with DHO response functions scaled by the Bose factor using the nominal frequency position. The Levenburg-Marquart algorithm was applied with ORIGIN 8.5 to obtain the best fit. The parameters of each successive lower temperature were initialized with the best -fit values of the previous higher-temperature results. This was continued down to 450 K and the goodness of fit χ^2 minima was used to determine the best fit. Fits were attempted with and without the four low-frequency peaks from 20 to 75 cm^{-1} at each temperature, but the end results showed the low-frequency peaks had zero amplitudes above 650 K, thus indicating they could not be resolved. Profiles from 450 to 600 K had significantly smaller χ^2 values when the low-frequency peaks were included, thus indicating their presence. At each temperature a fit of the broad CP was attempted with both a variable width and a fixed width set equal to the value found at 1000 K. The χ^2 result with variable width fits were consistently smaller and the parameters are shown in Fig. 8(a).

The lower-temperature profiles from 80 K upwards were similarly analyzed: The narrow CP was initialized first, followed by an arbitrary broad CP which was given a fixed width based on the 1000 K spectra and an amplitude that was set as large as possible while the remaining DHO peaks were then initialized with the Bose factor. Higher temperatures were fit using the final parameters of the previous lower temperature and care was taken to fix the DHO amplitudes above 100 cm^{-1} whenever possible, thus ensuring that most of the amplitude changes would be attributed to the CPs. Fits with variable broad CP widths were attempted but found not to be successful in that the parameter evolution of the low-frequency phonon modes were erratic. The decision to fix the broad CP width was also partly based on the results shown in KH_2PO_4 [49] and $Rb_{1-x}K_xCaF_3$ [50] where broad CPs are found to be temperature independent within each phase. It is important to note that, when fitting complex spectra such as those of NBT, the quality of the fit is necessary but not sufficient in determining the validity of the underlying model. It is also essential to examine the values obtained for the fitting parameters in the context of the particular physical phenomena studied as shown in a recent study of PZN [51]. It is often possible to obtain good fits with values of the fitting parameters that are not physically meaningful in this context, hence the decision to fit with a fixed broad CP width despite the possibility of higher goodness-of-fit values compared to a variable width.

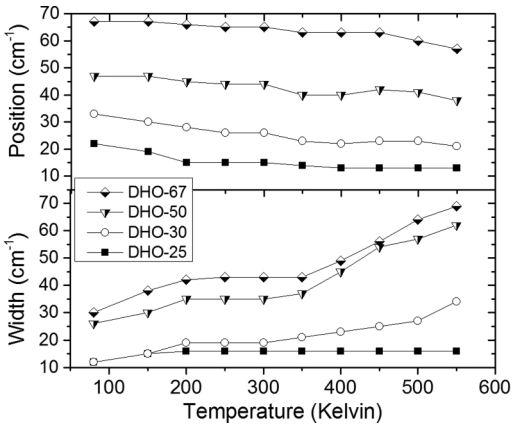

FIG. 9. Comparison of position and width of the four lowest-frequency phonon modes upon cooling. All peaks exhibit softening and damping near the 570 K transition. (a) Broad central peak, (b) Narrow central peak.

The analysis of the low-frequency part of the spectrum was more delicate, particularly at intermediate temperatures where both CPs overlap the four lowest-frequency peaks. A set of models were examined: The four low-frequency modes were allowed positions and widths that were either fixed or variable for only the lowest one, two, three, or all four at once. Additionally, the model by Axe and Shirane [52] where the CP is coupled to the lowest DHO phonon was considered as it reduces the number of parameters by one for each mode coupled. The use of this model did not substantially improve the fits and thus cannot be informative as to the underlying physics in this system, particularly as the four lowest phonon modes overlap so significantly. Four uncoupled modes with variable widths and positions yielded the lowest χ^2 value and the results are shown in Fig. 9. The phonon peak at 23 cm^{-1} is seen to change position and width up to 200 K, basically becoming Lorentzian in profile and fitting directly underneath the narrow CP. Adjustments of its parameters above 300 K did not result in any changes to the χ^2 value and its presence is assumed only on the basis of its existence at 80–150 K. The other three peaks slowly soften and dampen with increasing temperature up to 600 K, with an increase in damping above 350 K for the three higher phonons. Fits were not attempted above 600 K as the low-frequency peaks are not resolved from the broad CP as explained above.

Lorentzian fits instead of DHOs were also attempted for the high-frequency peaks in the cubic, tetragonal, and low-temperature phases, but were not retained as useful solutions because the χ^2 values were much higher than for DHOs, particularly at the lowest temperatures. The possibility of an anharmonic oscillator model was also not considered as the DHO fits were excellent at all temperatures above 100 K and there is no indication of a Fano-like line shape as reported in $BaTiO_3$ [53].

The Raman spectra analysis distinguishes between the higher-frequency peaks, corresponding to the hard modes, and the lower-frequency peaks and CPs. Comparing the experimental spectra at different temperatures, it is relatively easy to see that each main phonon peak is composed of two or more component peaks, as should be expected from symmetry considerations. According to the group theory analysis of Kreisel *et al.* [36], 15 Raman active modes are expected in the tetragonal phase and 13 in the rhombohedral phase. However, to minimize the number of fitting parameters, only two DHOs were used for each high-frequency phonon peak in the tetragonal phase and a good fit could still be obtained. The temperature-dependent results of the high-frequency modes were similar to those reported by Luo *et al.* [35] and are not reproduced here. The temperature evolution of the parameters of the low-frequency composite peak are shown in Fig. 9.

Figure 7 shows examples of the fitted spectra at 80, 400, 700, and 950 K, i.e., below the lower transition, between the two transitions, and above the higher transition. The main features that differentiate our results from the previous work by Luo [35], Siny [30], and Kreisel [36] is the inclusion of two CPs and fitting of the low-frequency composite peak near 40 cm^{-1} with four peaks.

Figures 8(b) and 8(a) show the fitting results for the CP parameters. The amplitudes of the two Lorentzian CPs exhibit different temperature dependencies. The narrow CP amplitude has a cusp-like maximum at 600 K, near the lower phase transition, and steadily decreases on either side to a minimum at the highest and lowest temperatures similar to the dielectric constant [17]. The narrow CP amplitude also has notable overlap between the two fitting models used in the region of 450–600 K despite having arrived at these values starting from two very different initial spectra. The broad CP amplitude profile is qualitatively similar to the total integrated intensity seen in Fig. 4, flat between 900 and 600 K with a steady decrease in the low-temperature range similar to the narrow CP amplitude. The width of the narrow CP decreases continuously with temperature and shows almost no anomaly at the lower phase transition. In the inset, the corresponding relaxation time in the high-temperature region is seen to follow a Vogel-Fulcher pattern. In contrast, the width of the broad CP decreases throughout the cubic phase and becomes flat in the tetragonal phase with a small increase at 600 K. The curves for the broad CP amplitude do not meet near 550 K due to the presence of the low-frequency peaks in the fits started from low temperature.

V. DISCUSSION

A. Central peaks

The present results on the CPs and low-frequency peaks represent the most original part of the present study. Previous reports [33] indicated that there was only one low-frequency peak and one CP. Only a qualitative estimate of the relaxation time from the width of the broad CP was given without deconvolution into two separate peaks although the possibility for two peaks was suggested. Consequently, the present study with a full deconvolution provides further and finer details on the transition dynamics of NBT. The Raman results for the CPs are shown qualitatively in Figs. 3(a) and 7 and quantitatively in Figs. 8(b) and 8(a). In the high-temperature range, 650 to 1000 K, the low-frequency region of the spectrum, 5–100 cm^{-1}, is fitted with two Lorentzians as it is impossible to resolve any low -frequency peaks. At the highest temperature, $T = 1000$ K, the central part of the spectrum seen in Fig. 3(a)

has a different overall shape from those at lower temperatures and it is primarily composed of a broad CP. Below the first transition at ≈820 K, two CPs can be distinguished, a narrow one and a broad one. Below the second transition at ≈570 K, three low-frequency phonon peaks emerge from the broad CP becoming four below 200 K. The analysis reveals that the CP spectrum cannot be fitted with a single Lorentzian profile at any temperature. It is also possible to speculate that the profile might be understood as one continuous distribution of relaxations potentially fitted with a single functional shape, but the two-Lorentzian approach shown below makes physical sense, allowing for separation of the central intensity into differing relaxation regions originating or related to two different physical mechanisms discussed below.

1. Broad central peak

Precursor ordering is common to order-disorder phase transitions [54] well above the phase transition temperature and occurs in NBT as rotations of anion octahedra diffuse to surrounding octahedra, lowering the space-group symmetry locally. The CP widths associated with precursor ordering correspond to fluctuation lifetimes while their amplitudes are related to the size or number of regions. These precursor regions can be modeled as asymmetric double well potentials involving rotations of the relatively rigid [48] TiO_6 anion octahedra [54,55], the rotation angle of which is the accepted order parameter in NBT [7]. The double well potential for the anion octahedra in NBT can be understood qualitatively by considering the greater attraction of an oxygen atom to either of the two neighboring Bi^{3+} atoms rather than the Na^{1+} atoms, with Bi^{3+} therefore acting as a driver of the TiO_6 rotation. Given sufficient thermal energy, the octahedron anions can "hop" over to an alternate configuration and thus reorient either a single octahedron or a local elastic region. Thermal fluctuations must therefore involve variations in the rotational angle and propagate in a diffusive manner as the octahedra are corner sharing. These diffusive fluctuations are expected to increase in amplitude and lifetime as the phase transition is approached, resulting in the growth of the precursor regions. The TiO_6 rotations also cause a change in the unit cell lattice parameters [4] resulting in localized strain. Adjacent or nearby regions will interact via these local strain fields through rotational-translational coupling. This coupling is prominent in molecular crystals such as CH_4 and KCN [56], but to our knowledge has not been invoked in perovskites. We speculate that the relatively larger CP widths in NBT correspond not to a single time scale, but to a distribution of relaxation times that include fast rotations of single octahedra, and slower rotations of both correlated chains (M-point rotation) and regions (R-point rotations), which have differing sizes and interact via strain. This suggestion may help resolve the current questions about the origin and mechanism of strain dynamics in NBT [40,41].

The amplitude and width of the broad CP are shown in Fig. 8(a) and follow the expected temperature evolution for dynamics of precursor regions near first-order phase transitions. Precursor regions typically appear far above these transitions, often at $T > T_c + 40$ K [48,51], exhibiting a small steady increase upon approach to the transition with an abrupt change at the transition. The presence of tetragonal phase precursor regions in NBT are observed as faint neutron superlattice reflections at the M-point of the Brillouin zone where they reveal cog-wheel rotations of the anion octahedron [6] and from second-harmonic-generated light revealing a lower local symmetry up to 900 K [7]. These superlattice reflections are present at 1000 K and increase steadily in magnitude upon approaching the 820 K phase transition [6] where they abruptly increase to a higher value that is nearly constant throughout the tetragonal phase. Therefore the large broad CP width at 1000 K can be attributed to fast lifetime fluctuations of the anion octahedra. The decrease in the peak width in the cubic phase therefore indicates a slowing down of these fluctuations towards the 820 K transition. Concurrently, the increase in amplitude of this peak reveals an increase in the size or amplitude of the fluctuations. The presence of precursor regions is also observed in Fig. 7 where the high frequency fits in the cubic phase at 950 K and the tetragonal phase at 700 K are notably similar, thus confirming that the Raman inactive F_{1u} phonons [32] become Raman active due to the local symmetry breaking by the precursor regions. This similarity also suggests that NBT has no significant second-order Raman scattering, unlike $SrTiO_3$ [55].

In the tetragonal phase, from 650 to 800 K in Fig. 8(a), the amplitude and width of the broad CP remain relatively constant, consistent with the M-point Bragg peak amplitude [6]. This indicates that the precursor regions have grown in size and number so that they are in contact with each other and are the dominant structural phase. The strain due to the octahedron rotations, observed with x rays to have a maximum axis ratio [5] of $\frac{c}{a} - 1 = 0.002$, are not large enough to suppress the local fluctuations. The polydomain nature of this phase suggests that the diffusive fluctuations will involve strain-mediated rotational diffusion between adjacent nanoscale domains.

In the low-temperature phase, there is a five-fold decrease in amplitude seen in Fig. 8(a) from 600 to 80 K, which is consistent with freezing of the dynamic fluctuations [54] and correlated with the appearance of the low symmetry, polar phase [10]. As mentioned in the results section, the change in the intensity ratio of the 295/35 peaks seen in Fig. 5 through the low-temperature phase suggests a change in the broad CP background. This intensity ratio is temperature independent above 600 K and shows a steady increase upon cooling to 80 K due to the broad CP amplitude decrease. The mechanism of the diffusive fluctuations from 600 to 400 K are now related to heterophase rotational diffusion between the coexisting R-point and M-point anion octahedral rotations observed in neutron [6] and x-ray results [11]. Below 400 K, the observation of nanometer scale tetragonal platelets and twinning [9] suggests that these strain-related rotational fluctuations can persist to lower temperatures.

To confirm this hypothesis, a comparison to other similar perovskite materials is considered. The width of the broad CP in NBT is comparable only to materials that exhibit rotational reorientation of molecular constituents with precursor ordering near the structural phase transitions. The previously mentioned fluoroperovskites, $KMnF_3$[57]($\Gamma_1 \approx$ 10–30 cm^{-1} and $\Gamma_2 \approx$ 120–170 cm^{-1} between $T_{c1} = 186$ K and $T_{c2} = 91.5$ K), $RbCaF_3$ ($\Gamma \approx 80$ cm^{-1} above $T_{c1} = 186$) [12] and its

potassium-doped solid solutions [50], all have comparable CP widths that are present far above the transition temperature and are constant within the noncubic structural phases. The precursor ordering above the phase transition also results in first-order Raman peaks, and octahedral rotation is the primary order parameter of their respective phase transitions. By contrast, none of the titanate perovskites have similar widths, nor do any of their *A*-site mixed derivatives such as $Pb_{0.6}Sr_{0.4}TiO_3$ [58], $Ba_xSr_{1-x}TiO_3$ [59], $Ba_xCa_{1-x}TiO_3$ [60],or $Pb_{1-x}Ba_xTiO_3$ [61]. There are few *A*-site disordered perovskites with well studied CPs available for comparison. Lead-based relaxors were also considered because of their disorder-based characteristics and the lone pair of electrons in the outer shell is similar to the configuration of the Bi^{3+} ion in NBT. However, the CPs in Pb relaxors were generally found to derive from different physical phenomena, namely an overdamped soft mode in PMN [62], transverse acoustic-transverse optic (TA-TO) coupling in PZN [51] and slow relaxations of polar regions in PST [63]. Based on these comparisons to other similar materials, we conclude that the physical origin of the broad CP in NBT is due to rotational diffusion of the anion octahedra.

2. Narrow central peak

The temperature evolution of the narrow CP amplitude can be explained by PND dynamics and, near the lower-temperature phase transition, overlap of the low-frequency phonon modes. Dynamical polar behavior has been observed in the dielectric relaxation spectrum [11,17] to increase with decreasing temperature smoothly through the 820-K phase transition to a maximum near the 570-K phase transition and then decrease in a monotonic fashion through the lower-temperature phase [17]. The narrow CP amplitude seen in Fig. 8(b) qualitatively follows this temperature progression in that it also increases without obvious changes through the 820-K phase transition to a single cusp at 600 K and decreases steadily down to 80 K. In the cubic-to-tetragonal phases the amplitude increase can therefore be attributed to the increasing size and number of PND's until 570 K, where the subsequent decrease is then due to freezing of the domains which become static and macroscopically large [10,19]. The presence of cation relaxation at all temperatures, far from the phase transitions and at low temperatures, is unusual and due to the small cation size on the *A*-site relative to the available space. The ^{23}Na reorientation observed in NMR [15] suggests that dynamical variations in dipole strength and direction are possible without complete polarization reversal. Although the eight-site potential model is well accepted for *B*-site cations such as Ti [48], there is no theoretical model to our knowledge about the local potential restrictions for the *A*-site cations, but they are expected to have an average position aligned with the *B*-site ion.

The cusp in the amplitude near 570 K is sharper than expected for the known dielectric response. Comparison of the dielectric relaxation peaks seen in NBT [17] to other typical relaxors such as KLT and PST [64] provides information on the nature of the local ordering of the PNDs. KLT and PST data indicate that strongly disordered systems exhibit broad dielectric peaks, while more ordered systems have a sharp drop at the transition temperature. There is more evidence of NBT being a disordered system with the lower phase transition spread over at least 100° [6], so the relatively sharp CP amplitude peak at 600 K, which does not follow the broad character of the dielectric relaxation profile, may be due to an additional component. A possible explanation is that the low-frequency phonons, which exhibit increased damping near the transition and soften so that they overlap the CP near 600 K, couple to the relaxations as symmetry considerations do not exclude this interaction. Similar low-frequency phonons are assigned as *R*-point phonons in both $KMnF_3$ and $RbCaF_3$ systems and are therefore expected to become Raman inactive above the transition. The presence of faint *R*-point neutron Bragg peaks [6] in the tetragonal phase suggest remnants of these phonons may continue to contribute to the narrow CP above 600 K, exhibiting increased damping that is associated with shorter phonon lifetimes [47], but are not resolvable in these measurements. It should also be noted that the temperature dependence of the narrow CP amplitude seen in Fig. 8(b) is nearly identical to that of the Brillouin CP integrated intensity [39] taken upon cooling, which would be expected as the total Brillouin spectra corresponds to $\pm 3\ cm^{-1}$, i.e., within the narrow CP.

The width of the narrow CP also follows the expected behavior for order-disorder phase transitions. Dielectric relaxations originating from PND fluctuations are generally recognized to follow the Vogel-Fulcher (VF) model for order-disorder transitions [19]. The VF model, $\tau = \tau_0 \exp^{\{U/[k(T-T_m)]\}}$, is used to describe freezing related to the growth of clusters of electric dipoles above a freezing temperature T_m. The narrow CP width in NBT appears linear in Fig. 8(b), but the inset shows the relaxation time from 1000 to 600 K following a VF model with an activation energy $\frac{U}{k} =$ 24 K, a freezing temperature T_m of 554 K and a relaxation time τ_0 of 2.09×10^{-12} s. This value for T_m is close to the known onset temperature of spontaneous remnant polarization [17]. Below T_m, the relaxation time from 600 to 150 K changes linearly with temperature with a slope of 7.45×10^{-9} s/K, which is also consistent with the monotonic evolution of the dielectric constant below 570 K [17] and the expected change in dynamics due to the onset of microscopic polar regions [10].

An alternate hypothesis that must be considered is a CP due to fluctuations resulting from defect mobility [65] as these are also known to be 3–15 cm^{-1} in width. Oxygen vacancy defects in NBT have been reported in conductivity measurements [42], crystal growth [66,67], and may be deduced in our sample from both the absorption spectrum and laser heating as shown in Figs. 2 and 1, respectively, as well as the presence of the faint Ti-O terminating mode at 1060 cm^{-1} attributed to vacancies [68] (data not shown). However, the defect concentration is expected to be less than one part per billion based on similar vacancy concentrations observed after vacuum annealing in other titanates [69]. Therefore the physical origin of the narrow CP is more likely to be the PND dynamics rather than defects based on the simple argument of the relative density of the two components. Also, defect mobility is not expected to have a peak at 600 K as mobility would increase with increasing temperature, thus affirming the correlation between the narrow CP amplitude peak at 600 K to the temperature evolution of the dielectric constant.

One can thus propose the following description of the transition dynamics in NBT. Above Tc_1 at 820 K, NBT is, on average, cubic, although the high-frequency phonon peaks and the broad CP both reveal the onset of precursor regions of tetragonal symmetry observed as the planar M-point rotations of the O_6 octahedra. The associated relaxations are related to thermally activated rotational diffusion and translational-rotational coupling. The relaxation time of these fluctuations increase with decreasing temperature in the cubic phase, with the broad CP becoming stable in the tetragonal phase while the narrow CP continues to decrease with a VF character to ∼554 K. These relaxations in the tetragonal phase are also accompanied by low-symmetry precursor phase formations as evidenced by R-point Bragg peaks as well as correlated fluctuations of the cation displacements which are responsible for the growth of the narrow CP and are confirmed by the characteristic relaxor behavior of the dielectric constant due to the formation of polar nanodomains in the same temperature range [17]. Finally, the low-temperature phase has a decrease in the amplitudes of both CP's and a linear decrease in the narrow CP width due to motional freezing of the cations, TiO_6 octahedrons, and the hardening of the low-frequency phonon modes.

B. Assignment and temperature evolution of the phonon peaks

The NBT Raman results are shown in Fig. 7, and as the high-frequency regions above 100 cm^{-1} have already been well described [30,35,36], the focus here is on the new low-frequency results. The fits reveal the presence of four peaks in the 5–100 cm^{-1} region below 150 K, which can be reduced to three above 200 K as the lowest-frequency peak becomes eclipsed by the narrow CP. In Fig. 9, the evolution of the phonon positions show definite softening behavior that is linear in ω vs. T, as well as increased damping near the lower phase transition. None of the attempted fits followed the ω^2 vs. T character reported previously for the composite peak [33]. This linear dependence is more characteristic of an order-disorder transition as per the Lyddane-Sachs Teller relation [70], and is consistent with the known characteristics of the lower-temperature phase transition and the monotonic evolution of the dielectric constant below 570 K [17]. The damping shows a sharp increase above 350 K, concurrent with the presence of mixed phases [6], further emphasizing the dynamic nature of the transition. The linear temperature dependence of the positions in Fig. 9 are also notably similar to the monotonic temperature evolution of the width and position of the low-frequency modes at 28, 37, 49, and 62 cm^{-1} in monoclinic $KMnF_3$ and 31, 36, 44, 75.6, and 84 cm^{-1} in orthorhombic $RbCaF_3$. By comparison, the previously mentioned oxide perovskites all have either one or two low-frequency modes which exhibit softening with an ω^2 vs temperature dependence upon approach to the cubic-to-tetragonal transition, and no significant change near the lower-temperature $R3c$ symmetry phases. In general, $R3c$ symmetry perovskite ferroelectrics such as $BiFeO_3$ [71] and $NaNbO_3$ [72], $R\bar{3}c$ symmetry perovskites such as LaAlO3 [73] and $LaCoO_3$ [74] all have either one or two modes in the low-temperature phase. The lack of correspondence between the low-frequency modes of NBT and any of either the oxide titanate perovskites or perovskites of $R3c$ and $R\bar{3}c$ symmetry suggests that the $R3c$ symmetry assignment may not be correct. The recent suggestion of Cc monoclinic symmetry [27] was made despite the admitted absence of a confirming peak at the [0.5,0.5,0.5] point of the Brillouin zone. This inconsistency, in conjunction with the low-frequency results shown here, suggests that additional work is required to determine the correct low-temperature symmetry. We also note that the temperature dependence of the lattice parameters determined from x-ray analysis are strikingly similar between NBT [5] and $KMnF_3$ [13], particularly in the low-temperature phases where the lattice parameters of $KMnF_3$ in the monoclinic phase are too similar to be resolved. Direct comparison to other perovskite materials of Cc symmetry is not possible at this time as we are unaware of any other perovskite materials with fitted low-frequency modes. PZT-PT [75–77] and thin films of $BiFeO_3$ [78] on $SrTiO_3$ substrates have been assigned Cc symmetry, but no deconvolution of low-frequency modes was attempted despite evidence of multiple peaks in the low-frequency region. These results in NBT appear to confirm the recent suggestions of a different low-temperature symmetry in NBT as there are more low-frequency modes than $R3c$ materials and these modes disappear concurrently with the R-point Bragg peak in neutron scattering [6]. However, the assignment of Cc cannot be confirmed due to the lack of polarization information for each peak.

VI. CONCLUSION

The Raman results of NBT presented in this paper have revealed the existence of two CPs, a narrow one and a broad one. Both peaks appear well above the high temperature cubic-tetragonal transition, but display very different temperature behavior. The broad CP clearly grows upon approach of the high-temperature transition (≈820 K), which is related to the cooperative rotations of oxygen octahedra (M point of the reciprocal lattice). Its origin is therefore the rotational fluctuations and their their diffusion, which are associated with the presence of precursor clusters of the tetragonal phase. By contrast, the narrow CP grows continuously through that transition and unaffected by it, as does the dielectric peak that corresponds to the relaxor behavior. The narrow CP is therefore associated with the same relaxational dynamics that give rise to the relaxor behavior of the dielectric constant. Upon crossing the low-temperature phase transition (≈580 K), both CPs progressively loose amplitude, indicative of a slowing down of their relaxational dynamics and the progressive establishment of a static long-range order, independently confirmed by x-ray measurements. Concurrently, four low-frequency phonons appear in the spectrum. Their number suggests a low-temperature ferroelectric phase different than the $R3c$ symmetry previously reported.

ACKNOWLEDGMENTS

The authors wish to thank Dwight Viehland for suggesting the NBT topic and providing support for part of the work through Subcontract No. CR-19384-477990 from NSF-MWN (Materials World Network) Grant No. DMR-0806592.

[1] T. Takenaka, H. Nagata, and Y. Hiruma, IEEE Trans. Ultrason. Ferroelectr. Freq. Control **56**, 1595 (2009).
[2] S. A. Sheets, A. N. Soukhojak, N. Ohashi, and Y.-M. Chiang, J. Appl. Phys. **90**, 5287 (2001).
[3] W. Ge, H. Liu, X. Zhao, W. Zhong, X. Pan, T. He, D. Lin, H. Xu, X. Jiang, and H. Luo, J. Alloys Compd. **462**, 256 (2008).
[4] A. M. Glazer, Acta Crystallographica Section A **31**, 756 (1975).
[5] J. A. Zvirgzds, P. P. Kapostin, J. V. Zvirgzde, and T. V. Kruzina, Ferroelectrics **40**, 75 (1982).
[6] S. Vakhrushev, B. Kvyatkovskii, R. Malysheva, N. Okuneva, E. Plachenova, and P. Syrnikov, Kristallografiya **34**, 154 (1989).
[7] G. Jones and P. Thomas, Acta Crystallogr. B **58**, 168 (2002).
[8] Y. Liu, R. L. Withers, J. Wang, L. Norén, A. J. Studer, and Y. Li, J. Adv. Dielectr. **02**, 1230012 (2012).
[9] V. Dorcet and G. Trolliard, Acta Mater. **56**, 1753 (2008).
[10] J. Yao, W. Ge, L. Luo, J. Li, D. Viehland, and H. Luo, Appl. Phys. Lett. **96**, 222905 (2010).
[11] J. Suchanicz, Ferroelectrics **200**, 319 (1997).
[12] P. Daniel, M. Rousseau, and J. Toulouse, Phys. Rev. B **55**, 6222 (1997).
[13] A. Ratuszna and A. Kachel, Acta Crystallographica Section B **48**, 118 (1992).
[14] H. Unoki and T. Sakudo, J. Phys. Soc. Jpn. **23**, 546 (1967).
[15] I. P. Aleksandrova, A. A. Sukhovsky, Y. N. Ivanov, Y. E. Yablonskaya, and S. B. Vakhrushev, Ferroelectrics **378**, 16 (2009).
[16] V. A. Shuvaeva, D. Zekria, A. M. Glazer, Q. Jiang, S. M. Weber, P. Bhattacharya, and P. A. Thomas, Phys. Rev. B **71**, 174114 (2005).
[17] C.-S. Tu, I. G. Siny, and V. H. Schmidt, Phys. Rev. B **49**, 11550 (1994).
[18] B. Tilak, Am. J. Mater. Sci. Technol. **2**, 110 (2012).
[19] R. Pirc and R. Blinc, Phys. Rev. B **76**, 020101 (2007).
[20] J. Harada, T. Pedersen, and Z. Barnea, Acta Crystallogr. A **26**, 336 (1970).
[21] G. Shirane, R. Pepinsky, and B. C. Frazer, Acta Crystallogr. **9**, 131 (1956).
[22] S. Takagi, A. Subedi, V. R. Cooper, and D. J. Singh, Phys. Rev. B **82**, 134108 (2010).
[23] K. Wang, J.-M. Liu, and Z. Ren, Adv. Phys. **58**, 321 (2009).
[24] M. W. Lufaso, P. W. Barnes, and P. M. Woodward, Acta Crystallographica Section B **62**, 397 (2006).
[25] C. J. Howard and H. T. Stokes, Acta Crystallographica Section B **54**, 782 (1998).
[26] J. Kreisel, A. M. Glazer, P. Bouvier, and G. Lucazeau, Phys. Rev. B **63**, 174106 (2001).
[27] S. Gorfman and P. A. Thomas, J. Appl. Crystallogr. **43**, 1409 (2010).
[28] E. Aksel, J. S. Forrester, J. L. Jones, P. A. Thomas, K. Page, and M. R. Suchomel, Appl. Phys. Lett. **98**, 152901 (2011).
[29] F. Cordero, F. Craciun, F. Trequattrini, E. Mercadelli, and C. Galassi, Phys. Rev. B **81**, 144124 (2010).
[30] I. Siny, E. Husson, J. Beny, S. Lushnikov, E. Rogacheva, and P. Syrnikov, Phys. B (Amsterdam, Neth.) **293**, 382 (2001).
[31] E. V. Balashova and A. K. Tagantsev, Phys. Rev. B **48**, 9979 (1993).
[32] J. Petzelt, S. Kamba, J. Fábry, D. Noujni, V. Porokhonskyy, A. Pashkin, I. Franke, K. Roleder, J. Suchanicz, R. Klein, and G. E. Kugel, J. Phys. Condens. Matter **16**, 2719 (2004).
[33] I. G. Siny, E. Husson, J. M. Beny, S. G. Lushnikov, E. A. Rogacheva, and P. P. Syrnikov, Ferroelectrics **248**, 57 (2000).
[34] M.-S. Zhang, J. F. Scott, and J. A. Zvirgzds, Ferroelectr., Lett. Sect. **6**, 147 (1986).
[35] L. Luo, W. Ge, J. Li, D. Viehland, C. Farley, R. Bodnar, Q. Zhang, and H. Luo, J. Appl. Phys. **109**, 113507 (2011).
[36] J. Kreisel, A. M. Glazer, G. Jones, P. A. Thomas, L. Abello, and G. Lucazeau, J. Phys. Condens. Matter **12**, 3267 (2000).
[37] S. Trujillo, J. Kreisel, Q. Jiang, J. H. Smith, P. A. Thomas, P. Bouvier, and F. Weiss, J. Phys. Condens. Matter **17**, 6587 (2005).
[38] D. Rout, K.-S. Moon, V. S. Rao, and S.-J. L. Kang, J. Ceram. Soc. Jpn. **117**, 797 (2009).
[39] A. I. Fedoseev, S. G. Lushnikov, S. N. Gvasaliya, P. P. Syrnikov, and S. Kojima, Phys. Solid State **51**, 1399 (2009).
[40] D. S. Keeble, E. R. Barney, D. A. Keen, M. G. Tucker, J. Kreisel, and P. A. Thomas, Adv. Funct. Mater. **23**, 184 (2013).
[41] E. Aksel, J. S. Forrester, J. C. Nino, K. Page, D. P. Shoemaker, and J. L. Jones, Phys. Rev. B **87**, 104113 (2013).
[42] W. Ge, H. Cao, J. Li, D. Viehland, Q. Zhang, and H. Luo, Appl. Phys. Lett. **95**, 162903 (2009).
[43] Seung-Eek Park, Su-Jin Chung, In-Tae Kim, and K. S. Hong, J. Amer. Ceram. Soc. **77**, 2641 (1994).
[44] T. G. Siny, T. A. Smirnova, and T. V. Kruzina, Soviet Physics: Solid State **33**, 110 (1991).
[45] D. A. Long, *The Raman Effect: A Unified Treatment of the Theory of Raman Scattering by Molecules* (John Wiley & Sons, London, 2001).
[46] A. Fontana, F. Rossi, G. Viliani, S. Caponi, E. Fabiani, G. Baldi, G. Ruocco, and R. D. Maschio, J. Phys. Condens. Matter **19**, 205145 (2007).
[47] W. Hayes and R. Loudon, *Scattering of Light by Crystals* (John Wiley & Sons, London, 1978).
[48] M. Lines and A. Glass, *Principals and Applications of Ferroelectrics and Related Materials* (Oxford University Press, New York, 2004).
[49] I. P. Kaminow and T. C. Damen, Phys. Rev. Lett. **20**, 1105 (1968).
[50] P. Daniel, J. Toulouse, and M. Rousseau, Eur. Phys. J.: Appl. Phys. **5**, 33 (1999).
[51] J. Toulouse, F. Jiang, O. Svitelskiy, W. Chen, and Z.-G. Ye, Phys. Rev. B **72**, 184106 (2005).
[52] G. Shirane and J. D. Axe, Phys. Rev. Lett. **27**, 1803 (1971).
[53] D. L. Rousseau and S. P. S. Porto, Phys. Rev. Lett. **20**, 1354 (1968).
[54] A. D. Bruce and R. Cowley, Adv. Phys. **29**, 219 (1980).
[55] A. D. Bruce, W. Taylor, and A. F. Murray, J. Phys. C **13**, 483 (1980).
[56] R. M. Lynden-Bell and K. H. Michel, Rev. Mod. Phys. **66**, 721 (1994).
[57] D. J. Lockwood and B. H. Torrie, J. Phys. C **7**, 2729 (1974).
[58] S. Leal, F. Pontes, E. Leite, E. Longo, P. Pizani, A. Chiquito, M. Machado, and J. Varela, Mater. Chem. Phys. **87**, 353 (2004).
[59] D. A. Tenne, A. Soukiassian, X. X. Xi, H. Choosuwan, R. Guo, and A. S. Bhalla, Phys. Rev. B **70**, 174302 (2004).
[60] T. H. Kim, S. Kojima, K. Park, S. B. Kim, and J.-H. Ko, J. Phys. Condens. Matter **22**, 225904 (2010).

[61] G. Burns and B. A. Scott, Solid State Commun. **9**, 813 (1971).
[62] H. Taniguchi, M. Itoh, and D. Fu, J. Raman Spectrosc. **42**, 706 (2011).
[63] F. J. S.G. Lushnikov and S. Kojima, Solid State Commun. **122**, 129 (2002).
[64] J. Toulouse, B. E. Vugmeister, and R. Pattnaik, Phys. Rev. Lett. **73**, 3467 (1994).
[65] F. Schwabl and U. C. Täuber, Phys. Rev. B **43**, 11112 (1991).
[66] K. Yamamoto, M. Suzuki, Y. Noguchi, and M. Miyayama, Jpn. J. Appl. Phys. **47**, 7623 (2008).
[67] J. B. Babu, G. Madeswaran, X. Chen, and R. Dhanasekaran, Materials Science and Engineering: B **156**, 36 (2009).
[68] X. Dong Meng, D. Zhi Wang, J. Hua Liu, and S. Yuan Zhang, Mater. Res. Bull. **39**, 2163 (2004).
[69] D. Smyth, *The Defect Chemistry of Metal Oxides* (Oxford University Press, New York, 2000).
[70] R. Blinc and B. Žekš, *Soft Modes in Ferroelectrics and Antiferroelectrics* (North Holland, Amsterdam, 1974).
[71] A. A. Porporati, K. Tsuji, M. Valant, A.-K. Axelsson, and G. Pezzotti, J. Raman Spectrosc. **41**, 84 (2010).
[72] S. J. Lin, D. P. Chiang, Y. F. Chen, C. H. Peng, H. T. Liu, J. K. Mei, W. S. Tse, T.-R. Tsai, and H.-P. Chiang, J. Raman Spectrosc. **37**, 1442 (2006).
[73] V. G. Sathe and A. Dubey, J. Phys. Condens. Matter **19**, 382201 (2007).
[74] A. Ishikawa, J. Nohara, and S. Sugai, Phys. Rev. Lett. **93**, 136401 (2004).
[75] R. S. Solanki, S. K. Mishra, A. Senyshyn, S. Yoon, S. Baik, N. Shin, and D. Pandey, Appl. Phys. Lett. **102**, 052903 (2013).
[76] A. G. Souza Filho, K. C. V. Lima, A. P. Ayala, I. Guedes, P. T. C. Freire, J. Mendes Filho, E. B. Araújo, and J. A. Eiras, Phys. Rev. B **61**, 14283 (2000).
[77] K. C. V. Lima, A. G. Souza Filho, A. P. Ayala, J. Mendes Filho, P. T. C. Freire, F. E. A. Melo, E. B. Araújo, and J. A. Eiras, Phys. Rev. B **63**, 184105 (2001).
[78] S. Prosandeev, I. A. Kornev, and L. Bellaiche, Phys. Rev. Lett. **107**, 117602 (2011).